Volume 27
Number 43
21 November 2025
Pages 22853–23500

PCCP

Physical Chemistry Chemical Physics

rsc.li/pccp

25 YEARS ANNIVERSARY

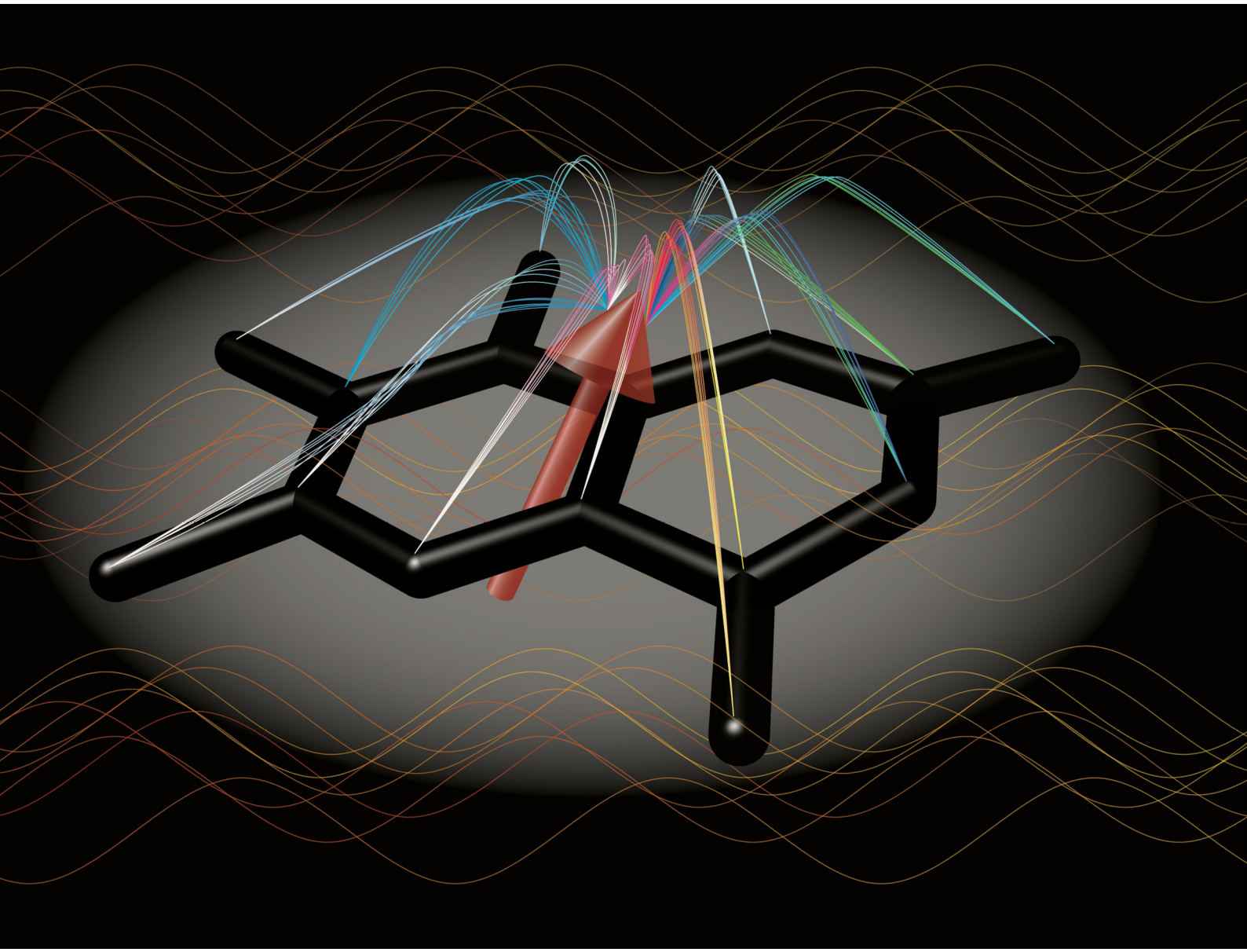

ISSN 1463-9076

ROYAL SOCIETY OF CHEMISTRY

PAPER

Stefan Weber *et al.*

Investigation of 6,7,8-trimethyllumazine and its radicals by NMR and photo-CIDNP spectroscopy

PCCP Owner Societies

PCCP

ROYAL SOCIETY OF CHEMISTRY

PAPER

View Article Online
View Journal | View Issue

Cite this: *Phys. Chem. Chem. Phys.*, 2025, **27**, 22911

Investigation of 6,7,8-trimethyllumazine and its radicals by NMR and photo-CIDNP spectroscopy

Sabrina Panter, [a] Boris Illarionov, [b] Jing Chen, [a] Adelbert Bacher, [c] Markus Fischer [b] and Stefan Weber *[a]

6,7,8-Trimethyllumazine (TML) is a structural analog of the natural cofactor 6,7-dimethyl-8-ribityl-lumazine. Under basic conditions, TML undergoes a distinctive disproportionation reaction upon photoexcitation. The transiently formed radical pair can be investigated by photo-chemically induced dynamic nuclear polarization (photo-CIDNP) spectroscopy. In this contribution, the structure of the TML anion is analyzed systematically using NMR spectroscopy. Furthermore, the transiently formed TML radicals are investigated and their hyperfine structures elucidated by ^{1}H and ^{13}C photo-CIDNP spectroscopy. Experimental photo-CIDNP intensities are compared with isotropic hyperfine coupling constants from density functional theory (DFT) calculations. The results confirm the formation of an oxidized TML$^{\bullet}$ radical and a reduced TMLH$^{\bullet-}$ radical, the latter potentially protonated at N1. Comparative analysis reveals a substantially different hyperfine structure of the formed radical species which is rationalized based on calculations of spin density distributions. The results provide important insights into photo-induced one-electron transfer reactions of 6,7-dimethyllumazines and their potential role in redox processes in biological systems. The detection and characterization of the oxidized TML$^{\bullet}$ radical is of special interest as this oxidation state has not been satisfactorily described in the literature so far. Thus this contribution advances the understanding of the mechanism of formation and the structure of lumazine radicals.

Received 4th June 2025,
Accepted 12th August 2025

DOI: 10.1039/d5cp02105g

rsc.li/pccp

1 Introduction

Lumazines are natural compounds found in various protein classes, although they are not as widely distributed as other essential coenzymes such as pterins or flavins.[1,2] The name "lumazine" originates from the strong fluorescence observed in unsubstituted lumazine,[3] see Fig. 1 for the structure. Intense fluorescence is a characteristic feature of many members of this compound class.[2] One particularly important member of lumazines is 6,7-dimethyl-8-ribityllumazine (DMRL, also abbreviated with DLZ). Like all 8-substituted 6,7-dimethyllumazines, DMRL exhibits a highly acidic 7α methyl group.[4,5] For DMRL and 6,7,8-trimethyllumazine (TML), the pK_A is reported as 8.3[6,7] and 9.9,[6–8] respectively. The proton exchange in aqueous solution is slow on the NMR timescale allowing both protonation states of DMRL and TML to be distinguished by NMR.[4,7,9,10] In basic solution, the structure of the anion has generally been described as a 7α-exomethylene moiety.[7,9] However, a recent study of TML conducted in our laboratories suggests that the TML anion is better described as a 7α-carbanion based on density functional theory (DFT) calculations of the singly occupied molecular orbital (SOMO) of the oxidized TML radical.[11] Due to the ribityl residue, DMRL additionally forms different five- and six-membered cyclic ethers in basic solution. The cyclic structures are formed from the DMRL anion under participation of hydroxy groups in the ribityl side chain.[7]

In nature, DMRL was first identified in 1966 as a direct biosynthetic precursor of riboflavin.[12] The final synthesis step, catalyzed by riboflavin synthase, involves the remarkable transfer of a four-carbon fragment between two DMRL molecules to form the riboflavin molecule.[13–15] The lumazine synthase/riboflavin synthase complex has been extensively studied in the context of antibiotic development, as their inhibition disrupts riboflavin biosynthesis in microorganisms, see *e.g.* ref. 16–20. Since 1978, DMRL has also been known to function as a chromophore in a protein thereafter named lumazine protein (LumP) from the marine bacterium *Photobacterium phosphoreum*. This protein was found to form a complex with the fluorescent protein luciferase.[21,22] The complex exhibits a blue-shifted bioluminescence due to Förster resonance energy transfer from luciferase to DMRL, as well as an increased quantum yield compared to

[a] *Institut für Physikalische Chemie, Albert-Ludwigs-Universität Freiburg, Albertstr. 21, 79104 Freiburg, Germany. E-mail: stefan.weber@pc.uni-freiburg.de*
[b] *Institut für Lebensmittelchemie, Universität Hamburg, Grindelallee 117, 20146 Hamburg, Germany*
[c] *TUM School of Natural Sciences, Technische Universität München, Lichtenbergstr. 4, 85747 Garching, Germany*

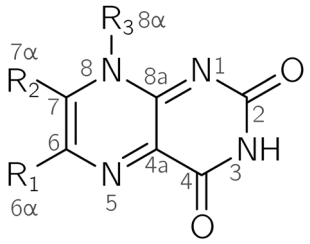

Fig. 1 Structure of lumazines: lumazine: $R_1 = R_2 = R_3 = H$; 6,7-dimethyl-8-ribityllumazine: $R_1 = R_2 = CH_3$, R_3 = ribityl; 6,7,8-trimethyllumazine: $R_1 = R_2 = R_3 = CH_3$.

unbound luciferase.[23,24] Furthermore, DMRL has been identified as an additional cofactor in a recently discovered subgroup of the photolyase/cryptochrome family which is involved in *e.g.* DNA repair[25] and various light-driven biological responses.[26] In the FAD-binding protein cryptochrome B (CryB) from *Rhodobacter sphaeroides*, DMRL is located in the antenna-binding domain and broadens the absorbance section of the protein.[27] Further investigation of another member of the photolyase/cryptochrome subgroup, the (6-4) photolyase protein B (PhrB) from *Agrobacterium tumefaciens*,[28] indicates that DMRL plays a role surpassing the one of a simple antenna chromophore in this protein: DMRL evidently acts as a "photoprotective pigment" coupling the oxidation of the FAD cofactor with the reduction of DMRL under intense illumination.[29]

In general, lumazines can mediate one- and two-electron transfer reactions, as demonstrated by cyclovoltammetry with unsubstituted lumazine.[30] This makes three oxidation states accessible: the oxidized lumazine, the one-electron reduced lumazine radical and the fully reduced lumazine. In this regard, they share a similar redox reactivity as flavins, which can access the same biologically relevant oxidation states.[31]

The first optical absorption spectra of lumazine radicals in aqueous solution were obtained using pulse radiolysis.[32] Several studies have confirmed the formation of lumazine radicals in protein environment. DMRL bound to flavodoxin forms a radical upon dithionite titration.[33] A 6,7-alkylated 5-ribityllumazine (6,7-(2,3-dimethylbutano)-*N*(8)-ribityllumazine-5′-monophosphate) generated an anionic radical bound to old-yellow enzyme under reduction with dithionite.[34] Paulus *et al.* studied the wildtype lumazine protein from *Photobacterium leiognathi* as well as several mutants with DMRL and riboflavin as cofactors employing time-resolved absorption spectroscopy and derived kinetics of their photoreduction.[35]

Data on the lumazine radical obtained by magnetic resonance spectroscopy are scarce. Ehrenberg *et al.*[36] conducted the first continuous-wave electron paramagnetic resonance (cw-EPR) study on DMRL and several derivatives at room temperature under acidic conditions. Amongst others, hyperfine couplings of a cationic TML radical protonated at N1 and N5 were reported.[36] Westerling *et al.* later studied different 5-alkylated 5,6,7,8-tetrahydrolumazine radicals using cw-EPR at room temperature.[37] The aforementioned study by Paulus *et al.* included cw-EPR and electron nuclear double resonance (ENDOR) data on the DMRL radical bound to lumazine protein. The authors were able to determine the *g* factor as well as several hyperfine couplings of the neutral DMRL radical protonated at N5. This study highlights that DMRL can in principle act as a redox-active cofactor.[35]

The study of TML by Wörner *et al.*[11] conducted in our laboratories focused on a disproportionation reaction between neutral (TMLH) and anionic (TML^-) TML molecules, a photo-induced reaction involving a one-electron transfer process. Thus, a triplet-born, spin-correlated radical pair (SCRP) comprising an oxidized radical $TML^\bullet$ and a reduced radical $TMLH^{\bullet-}$ is formed. The oxidized radical $TML^\bullet$ corresponds to an oxidation state of lumazines previously unknown. It is only mentioned in a contribution by Tu and coworkers,[38] who give the redox potential of the one-electron oxidation of TML in acetonitrile without providing a valid reference. This oxidation state is analogous to a "superoxidized" flavin radical,[39,40] that is accessible through one-electron oxidation of the flavin with strong oxidants such as tetranitromethane or sulfate radical.[41] The rather harsh conditions of synthesis indicate that this oxidation state has no biological relevance. Thus, the first detection and characterization of $TML^\bullet$ by Wörner *et al.* expand the redox chemistry of lumazines to a fourth oxidation state, which unlike the respective flavin redox state is readily accessible simply by irradiation with light. Furthermore, DFT calculations suggest that $TMLH^{\bullet-}$ may be protonated at N5 in a subsequent step following radical pair formation to yield $TMLH_2^\bullet$ (N5). Proton hyperfine couplings of the 6α and 8α methyl groups of both radical species have been determined in the contribution.

This study employed photo-chemically induced dynamic nuclear polarization (photo-CIDNP) spectroscopy to investigate the transiently formed TML radicals.[11] Photo-CIDNP spectroscopy is a NMR technique that enables the indirect detection of short-lived SCRPs, offering an alternative to EPR techniques. This is achieved by probing the diamagnetic products of the SCRP which contain the fingerprint of the SCRP's electronic structure; for recent reviews on solution-state photo-CIDNP see ref. 42–44. Photo-CIDNP, established in 1967 by Bargon, Fischer and Johnsen[45,46] as well as Ward and Lawler,[47] is based on a combination of two aspects: (i) the fate of a photo-induced SCRP is multiplicity-dependent and (ii) the SCRP undergoes singlet–triplet-mixing with the mixing frequency being dependent on the difference of *g* factors of both radicals and the isotropic hyperfine coupling constants A_{iso}. This dynamic interplay leads to a spin-sorting process which manifests itself in hyperpolarized nuclear spin resonances of the diamagnetic product. When employing a time-resolved photo-CIDNP technique, the relative size of enhancement for each nucleus is proportional to its A_{iso} in the transient radical.

With this contribution, we aim to further characterize the radical states of TML, especially in light of the detection of a formerly unknown oxidation state in the lumazine realm. Given the emerging evidence for the role of DMRL in light-induced redox reactions within protein environments,[29] a detailed investigation of one-electron reduced and oxidized 6,7-dimethyllumazine radical states will provide crucial insights into lumazine redox reactivity. We chose TML over DMRL for two

reasons: its unique disproportionation reaction allows convenient access to two TML radical species. Additionally, the formation of multiple anionic structures of DMRL in basic solution complicates analogous disproportionation reactions. Previous publications mentioned an enhanced photodegradation of free DMRL in solution[33,35,48] which renders this molecule an unsuitable candidate for the characterization of its radical state in solution.

This study characterizes radicals formed from TMLH and TML^- using ^1H and ^{13}C photo-CIDNP spectroscopy. By comparing experimental A_{iso} values with values from DFT calculations, we determine the protonation states of the reduced and oxidized radical species. Together with previous work by Wörner *et al.*,[11] we provide a more complete understanding of the photo-induced disproportionation reaction of TML and the electronic structure of the oxidized TML radical. Additionally, we conduct a systematic structural analysis of TML^- in basic solution using (^1H,^1H)-NOESY spectroscopy to clarify the structure of the anion.

2 Experimental

2.1 Sample preparation

D_2O (99.9%) was purchased from Sigma-Aldrich (Saint-Louis, MO, USA). NaOH (99.9%) was purchased from Fisher Chemicals (Loughborough, UK). 6,7,8-Trimethyllumazine and [6,6α,7,7α-$^{13}C_4$]6,7,8-trimethyllumazine were purified by high-pressure liquid chromatography (HPLC) (LiChrospher, RP-18 column, 18 mm × 20 mm) using a 12–30% gradient of methanol in water (retention rate: 18 min, flow rate: 10 mL min^{-1}). The compounds were dissolved in water. D_2O was added as detailed with the respective experiment. Concentrations of samples of the neutral TMLH were determined by absorption spectroscopy using an extinction coefficient of 12 022 M^{-1} cm^{-1} at 404 nm.[8] The pH was adjusted by addition of small amounts of NaOH. The ratio of neutral to anionic TML^- was subsequently determined by ^1H NMR spectroscopy.

2.2 NMR and photo-CIDNP spectroscopy

All NMR and photo-CIDNP experiments were performed on a 14 T Avance III HD NMR spectrometer (Bruker, Ettlingen, Germany). An inverse TXI triple resonance probe head was used for NOESY experiments as well as ^1H NMR standard and photo-CIDNP experiments. For ^{13}C NMR standard and photo-CIDNP experiments a BBFO broadband probe head was used. The experiments were performed at 293 K. The NOESY experiment was performed using a standard phase sensitive pulse program with water suppression using excitation sculpting with gradients.[49] A mixing time of 550 ms was used. The data were processed using a *q*-sine function in both dimensions and line broadening of 1.00 Hz and 0.30 Hz in the direct and indirect dimension, respectively. The ^1H photo-CIDNP experiments were performed as described in ref. 50 except for a relaxation delay of 5 s instead of 10 s. For the ^{13}C photo-CIDNP experiments, the description in ref. 51 was followed except for a relaxation delay of 10 s instead of 30 s. The spectra were gained by Fourier transformation with line broadening of 3 Hz (^1H spectra) and 5 Hz (^{13}C spectra).

2.3 Computational methods

DFT calculations were carried out with ORCA (version 4.0).[52,53] For the input structure, six water molecules were placed around 6,7,8-trimethyllumazine to simulate the first solvation shell,[54] see Fig. S1 for the structure. Geometry optimizations were performed with the B3LYP functional,[55] the TZVP basis set[56] along with the def2/J auxiliary basis set[57] and the cpcm model.[58] Mulliken spin populations and isotropic hyperfine coupling constants were calculated using the B3LYP functional and the EPR-II basis set.[59] For the relaxed potential surface scan, an optimized structure of 6,7,8-trimethyllumazine was used. The angle of H7α′–C7α–H7α″ was varied from 102° to 120° in 37 steps. The calculation was conducted with the B3LYP functional and a SVP basis set.[56]

3 Results & discussion

3.1 Structure of the TML anion

In this contribution, NMR data were obtained from samples dissolved in H_2O. Consequently, the signals of the exchangeable 7α methyl groups are visible without any indication of line broadening, suggesting that the proton exchange occurs very slowly on the NMR timescale. The addition of a small amount of D_2O is required for technical purposes. For TML^-, two distinct signals (denoted H7α′ and H7α″) attributed to two H7α protons are discernible in 1D proton spectra (see Fig. S3 depicting a ^1H NMR spectrum of TML in aqueous solution at pH 10.4). This observation indicates a rigid structure of the C7–C7α bond.

To the best of our knowledge, no 2D data of TML^- detailing its structure are available in the literature. Therefore, a (^1H,^1H)-NOESY experiment of TML in basic solution was employed, see Fig. 2 for the resulting data and the structure of TML^-. It is notable that only two cross peaks of 7α protons are visible, between H6α and H7α′ as well as between H8α and H7α″. This clearly indicates that the structure resembles an exomethylene or that the rotation around the C7–C7α bond is very slow on the NMR time scale. For a carbanion, additional NOESY cross peaks between H6α and H7α″ as well as between H8α and H7α′ would be expected.

To test whether temperature-dependent rotational dynamics affect the two H7α resonances, we conducted 1D ^1H experiments within a temperature range of 283–333 K, see Fig. S4. The H7α′ and H7α″ resonances are gradually shifted to higher chemical shifts until H7α′ overlaps with the not fully suppressed H_2O signal. Line broadening or other indications of coalescence between both H7α signals are not observed, thus suggesting a rigid exomethylene structure.

Exomethylene and carbanion structures are expected to have different H7α′–C7α–H7α″ angles. A relaxed potential energy surface scan of TML^- was performed by varying the H7α′–C7α–H7α″ angle from 102° to 120°. The resulting data, as

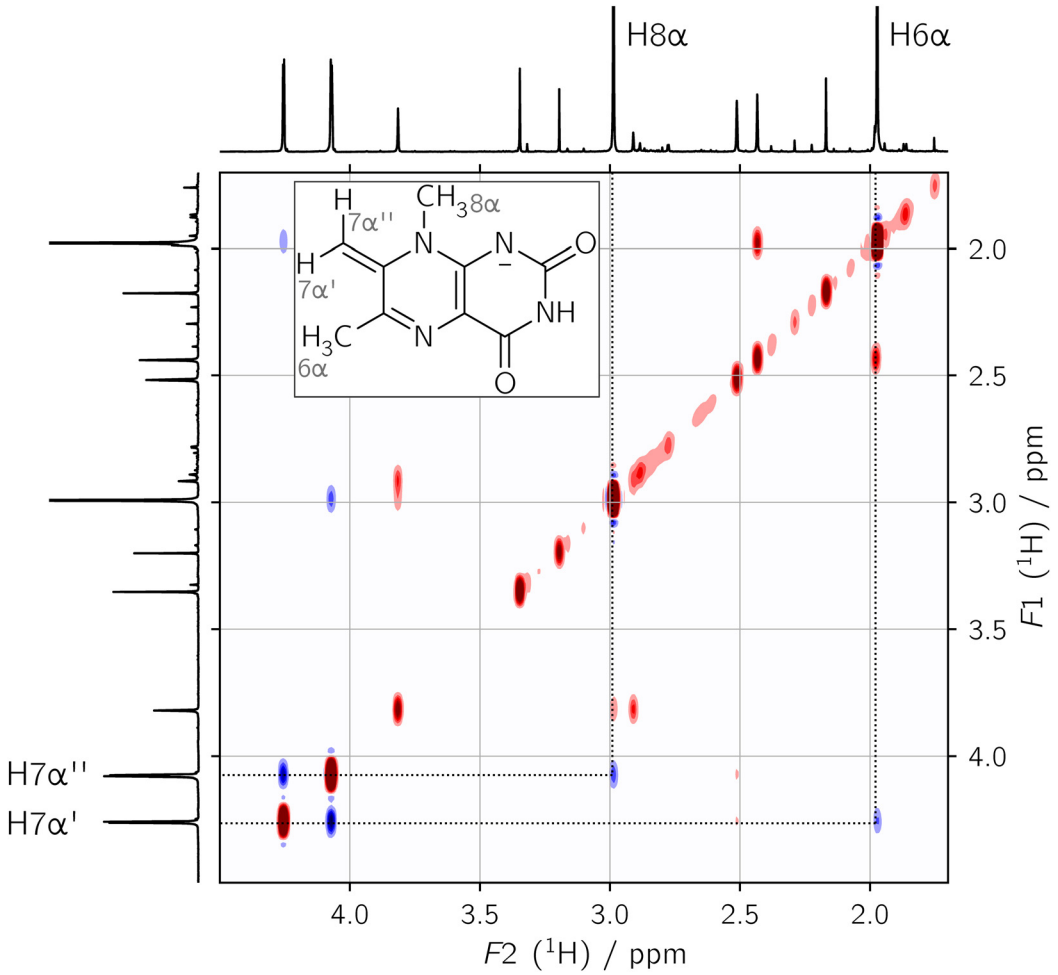

Fig. 2 (^{1}H,^{1}H)-NOESY spectrum of TML (6.0 mM) in a mixture of H_2O and D_2O (98.5 : 1.5, v/v) at pH 10.9. Cross peaks of the 6α and 8α methyl groups and the 7α protons in TML^- are marked by vertical and horizontal lines. Signals originating from neutral TML are not marked. For the experiment, 8 scans were accumulated.

depicted in Fig. S5, show one energy minimum at 117°. This value corresponds to the angle of a slightly distorted sp^2-hybridized carbon, which has a typical angle of 120°. The absence of a local minimum at around 109° indicates that a carbanion structure is energetically unfavorable.

The data presented do not indicate a carbanion structure, as the H7α resonances are well separated and demonstrate no sign of temperature-dependent coalescence. The NOESY data provide clear evidence that the structure of TML^- is not dynamic. Consequently, previous findings[11] must be reevaluated. The discussion of the authors is based on the SOMO of the $TML^\bullet$ radical which provides insight into the electronic structure with a high electron density at C7α. The binding situation of the diamagnetic TML^- molecule clearly does not reflect this.

3.2 Photo-CIDNP of TML

The previous photo-CIDNP study[11] discusses the relative A_{iso} values of H6α and H8α. To further characterize the hyperfine structure of the radical species formed during the photo-induced disproportionation reaction of TMLH and TML^-, a sample dissolved in a mixture of H_2O and D_2O (98.5 : 1.5, v/v) was used. The preparation of the sample in H_2O gives access to the photo-CIDNP signals of the 7α methyl group in both TML^- and TMLH. A highly homogeneous magnetic field is necessary for sufficient suppression of the H_2O signal given the proximity of both H7α′ and H7α″ resonances (4.0–4.4 ppm) to the H_2O signal. Fig. 3 illustrates the dark NMR spectrum (orange) and the transient photo-CIDNP spectrum (blue) of the prepared sample at pH 12.7. Both H7α′ and H7α″ protons exhibit strong absorptive resonances similar to H7α of TMLH. The resonance of intermediate intensity attributed to H8α of TMLH is absorptive as well. The remaining protons exhibit emissive resonances of strong (H6α of TML^-), average (H8α of TML^-) and weak (H6α of TMLH) intensity. The observed photo-CIDNP pattern is in accordance with previous findings[11] with the exception of H6α of TMLH. Wörner *et al.* did not detect a photo-CIDNP signal for this methyl group and attributed a relative photo-CIDNP intensity of 0. However, we were able to accumulate enough scans before photodegradation so that the photo-CIDNP signal of 6α protons is clearly visible. Comparing the photo-CIDNP signal patterns of H6α and H8α of TML^- and

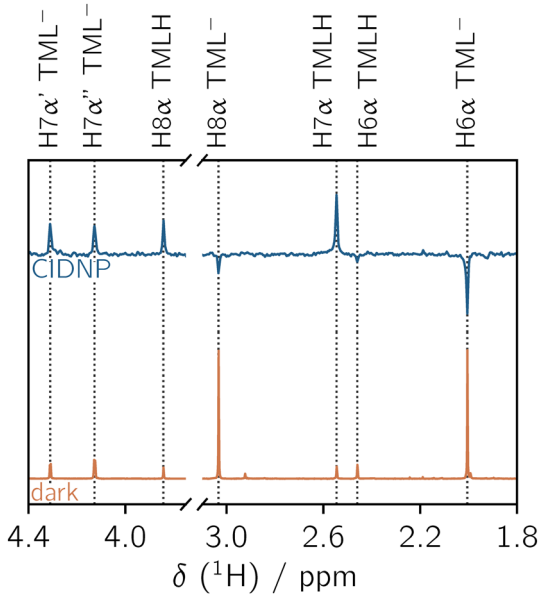

Fig. 3 Dark NMR (orange) and transient photo-CIDNP (blue) spectra of TML (1.6 mM) in a mixture of H_2O and D_2O (98.5 : 1.5, v/v) at pH 12.7. The ratio of TMLH : TML^- is 1 : 7. The dark NMR and photo-CIDNP spectra were measured with 16 and 256 scans, respectively. The sample was irradiated at 425 nm with 4.2 mJ.

Table 1 Absolute ^1H and ^{13}C hyperfine couplings of the reduced ($TMLH^{\bullet-}$, $TMLH_2^\bullet$ (N1), $TMLH_2^\bullet$ (N5)) and oxidized ($TML^\bullet$) TML radical species calculated using DFT (B3LYP/EPR-II). A_{iso} of protons in methyl groups are averaged, as a fast rotation is expected

	A_{iso}(abs)/MHz			
Nucleus	$TML^\bullet$	$TMLH^{\bullet-}$	$TMLH_2^\bullet$ (N1)	$TMLH_2^\bullet$ (N5)
H6α	15.10	−5.31	−5.37	1.67
H7α′	34.12			
H7α″	−34.51			
H7α		29.15	30.55	21.73
H8α	6.20	15.52	14.48	19.13
C6	24.84	−28.57	−29.25	−15.51
C6α	−8.07	0.69	1.00	−1.60
C7	−34.12	27.25	30.85	12.41
C7α	39.43	−14.28	−14.94	−9.82

TMLH reveals significant deviations of intensity and sign. This finding indicates a substantial shift in the hyperfine structure between the oxidized and reduced radical species.

As the source of photo-CIDNP polarization, Wörner *et al.*[11] proposed a redox cycle comprising photoexcitation of TMLH followed by single-electron transfer from the anionic TML^- to TMLH. Comparison of relative photo-CIDNP intensities with DFT calculations of A_{iso} suggested a subsequent protonation of the reduced $TMLH^{\bullet-}$ species at N5, thereby forming a transient $TMLH_2^\bullet$ radical species. Protonation of N1 was ruled out. The photo-CIDNP data presented in this contribution were analyzed in a similar way. To perform a linear correlation of the photo-CIDNP intensities with absolute A_{iso} values, we relied on DFT calculations as experimental data on the hyperfine couplings of TML radicals are scarce. The resulting A_{iso} values for the relevant nuclei are listed in absolute values in Table 1. The relative photo-CIDNP intensities from Fig. 3 were determined by integration and normalization to the most intense resonance arising from H7α′. These values are listed in Table 2, along with relative A_{iso} as determined by DFT for better comparability.

The linear correlation of the relative photo-CIDNP intensities of TML^- with $A_{iso}(TML^\bullet)$ is demonstrated in Fig. 4(a). A high correlation with a coefficient of determination of R^2 = 0.9860 as well as a slope m of −0.0278 MHz^{-1} was found. It is noteworthy that the correlation is marginally lower than the R^2 of 0.9996 reported by Wörner *et al.*,[11] which is to be expected with two additional data points. Still, the correlation remains remarkably high, substantiating the conclusion that this radical species is indeed formed as part of the transient SCRP. In a similar manner, linear correlations were performed of the relative photo-CIDNP intensities of TMLH with A_{iso} of the reduced radical species $TMLH^{\bullet-}$, $TMLH_2^\bullet$ (N1) and $TMLH_2^\bullet$ (N5), see Fig. 4(b)–(d). For $TMLH^{\bullet-}$ a high correlation with R^2 = 0.9745 was found (m = 0.0222 MHz^{-1}). Similar values were calculated for $TMLH_2^\bullet$ (N1): R^2 = 0.9884 and m = 0.0218 MHz^{-1}. However, R^2 = 0.7512 obtained from the correlation of $TMLH_2^\bullet$ (N5) is poor, which stands in contrast to the findings reported by Wörner *et al.*[11] DFT calculation of A_{iso}(H6α) predicts a positive value for $TMLH_2^\bullet$ (N5), contrasting with the negative sign predicted for both $TMLH^{\bullet-}$ and $TMLH_2^\bullet$ (N1). This additional

Table 2 Relative ^1H and ^{13}C hyperfine couplings of the oxidized and reduced TML radical species obtained from DFT calculations (B3LYP/EPR-II) and photo-CIDNP experiments. All experimental and theoretical values are normalized to H7α′ and C7α of $TML^\bullet$. Relative A_{iso} of $TML^\bullet$ obtained from photo-CIDNP are multiplied by −1 according to Kaptein's rule.[60] A_{iso} of protons in methyl groups are averaged, as a fast rotation is expected

	A_{iso}(rel) (DFT)	A_{iso}(rel) (CIDNP)	A_{iso}(rel) (DFT)			A_{iso}(rel) (CIDNP)
Nucleus	$TML^\bullet$	TML^-	$TMLH^{\bullet-}$	$TMLH_2^\bullet$ (N1)	$TMLH_2^\bullet$ (N5)	TMLH
H6α	0.44	0.53	−0.16	−0.16	0.05	−0.08
H7α′	−1.00	−1.00				
H7α″	−1.01	−0.87				
H7α			0.85	0.90	0.64	0.69
H8α	0.18	0.14	0.45	0.42	0.56	0.28
C6	−0.63	−0.61	−0.72	−0.74	−0.39	−0.44
C6α	0.20	0.17	0.02	0.03	−0.04	0.00
C7	0.87	0.57	0.69	0.78	0.31	0.49
C7α	−1.00	−1.00	−0.36	−0.38	−0.25	−0.15

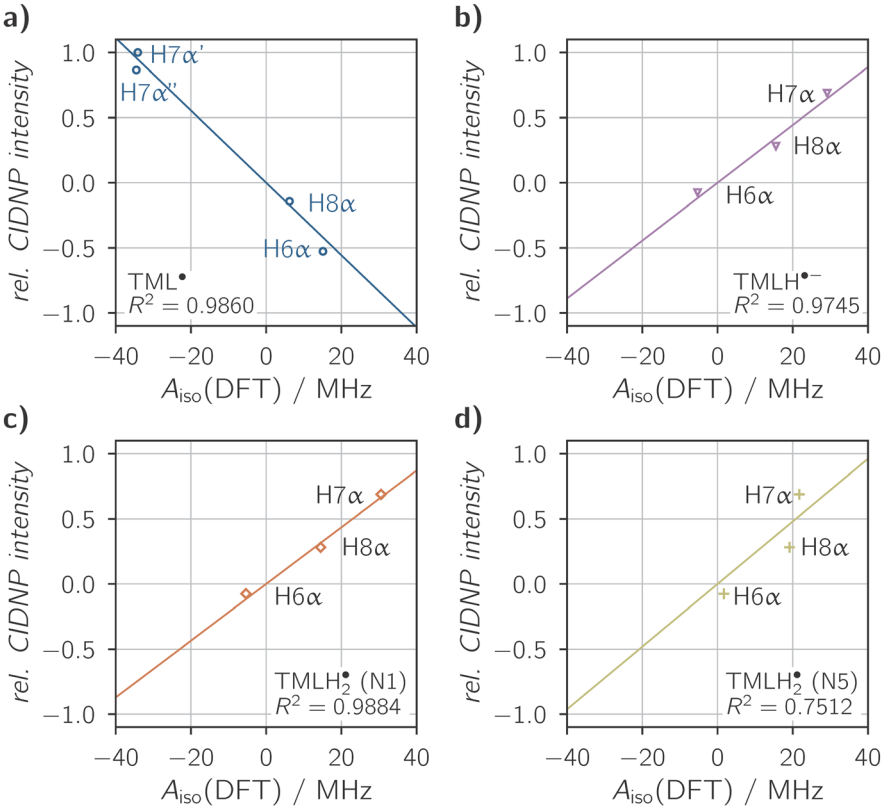

Fig. 4 Linear correlations of the experimentally determined relative ^{1}H photo-CIDNP intensities of TML^- and TMLH with calculated A_{iso} values of the corresponding radical species: (a) $TML^•$ (R^2 = 0.9860, m = −0.0278 MHz^{-1}), (b) $TMLH^{•-}$ (R^2 = 0.9745, m = 0.0222 MHz^{-1}), (c) $TMLH_2^•$ (N1) (R^2 = 0.9884, m = 0.0218 MHz^{-1}) and (d) $TMLH_2^•$ (N5) (R^2 = 0.7512, m = 0.0240 MHz^{-1}). The relative photo-CIDNP intensities of TML^- are negatively proportional to the respective hyperfine coupling according to Kaptein's rule.[60]

data point of H6α leads to a substantial decrease in R^2. Furthermore, as visible in Fig. 4(b)–(d), H7α exhibits a higher photo-CIDNP intensity than predicted by DFT calculations for $TMLH_2^•$ (N5). The combined contributions of these resonances result in a more refined hyperfine pattern for the reduced TMLH radical species. Consequently, we can eliminate $TMLH_2^•$ (N5) as a potential source of photo-CIDNP polarization. The distinction between $TMLH^{•-}$ and $TMLH_2^•$ (N1) remains difficult based on ^{1}H photo-CIDNP alone as both radicals share a comparable proton hyperfine coupling pattern and thus a similarly high correlation with DFT predictions.

A simple rule established by Kaptein[60] correlates the sign of photo-CIDNP enhancement with the sign of A_{iso}, the sign of Δg of the SCRP, the multiplicity of the SCRP's precursor and the reaction route of the SCRP. For two radicals of the same SCRP, Δg changes its sign. This results in a negative proportionality of A_{iso} and photo-CIDNP enhancement for nuclei in the oxidized TML radical while nuclei in the reduced TML radical exhibit a positive proportionality, compare Fig. 4(a)–(d).

The information obtained from ^{1}H photo-CIDNP experiments is limited, as merely four and three distinct protons are available for the oxidized and reduced TML radical species, respectively. However, the use of ^{13}C-labeled TML isotopologues can give access to the ^{13}C hyperfine structure, thereby providing more detailed insights into the radical species. An isotopologue that is both readily available and inexpensive (in terms of costs and synthesis efforts) is [6,6α,7,7α-$^{13}C_4$]6,7,8-trimethyllumazine.

The ^{13}C resonances of [6,6α,7,7α-$^{13}C_4$]TML^- and [6,6α,7,7α-$^{13}C_4$]TMLH were assigned according to (^{1}H,^{13}C)-HSQC data, see Fig. S6, and the splitting pattern of the ^{13}C resonances in the ^{13}C spectrum, see Fig. S7 for spectra at pH 7 and pH 13. The transient photo-CIDNP spectrum of [6,6α,7,7α-$^{13}C_4$]TML at pH 13 is depicted in Fig. 5. TML^- shows prominent emissive signals for both C7α and C6. C6α and C7 exhibit weaker absorptive resonances. From TMLH, signals attributed to C6 and C7α are clearly visible as emissive resonances. C7 shows a weaker absorptive resonance. A photo-CIDNP signal arising from C6α was not observed, which is in accordance to predictions of A_{iso} by DFT ranging from 0.69 MHz to 1.60 MHz, see Table 1. Comparison of the relative photo-CIDNP signals reveals that both radicals are easily distinguishable: $TML^•$ exhibits a strong hyperfine coupling for C7α, followed by C7 and C6. Only a weak hyperfine coupling is attributed to C6α. For reduced TML radical species, the strongest hyperfine couplings are found for C6 and C7. The hyperfine coupling of C7α is significantly weaker. This indicates a substantially different ^{13}C hyperfine pattern, a finding consistent with the previously discussed ^{1}H photo-CIDNP experiment.

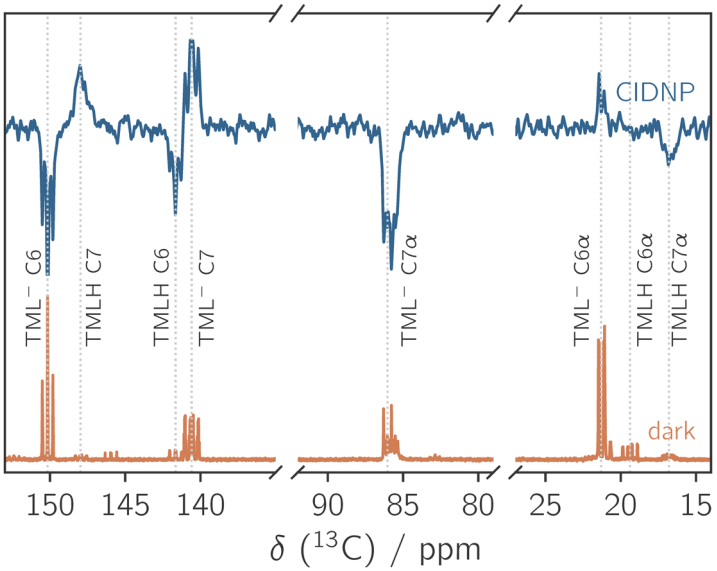

Fig. 5 Dark NMR (orange) and transient photo-CIDNP (blue) spectra of [6,6α,7,7α-$^{13}C_4$]TML (4.00 mM) in a mixture of H_2O and D_2O (30 : 70, v/v) at pH 13.0. The ratio of TMLH : TML^- is 1 : 8. For the sample preparation, a higher amount of D_2O was used to ensure a better lock signal and thus a better magnetic-field homogeneity. The signal of deuterated C7α is slightly shifted compared to the protonated C7α due to the heavy-atom effect. For the dark and photo-CIDNP spectra 20 480 and 10 752 scans, respectively, were accumulated. The sample was irradiated at 425 nm with 9.1 mJ.

The relation $|A_{iso}(7\alpha)| > |A_{iso}(6\alpha)|$ is found for the reduced TML radical in ^1H and ^{13}C photo-CIDNP although the sign of A_{iso} is inverted when switching from ^1H to ^{13}C. Heller, Chesnut and McConnell elucidated that for π-based radicals, the hyperfine coupling interaction of both α- and β-standing atoms depend on the spin population at the atom.[61,62] This relation accounts for the similarity in the size relations of 6α and 7α nuclei. In both cases, the transfer of spin density from the atom in the π system to the substituents occurs through polarization of σ-bonds. The mechanism of spin density transfer is direct polarization for α substituents and hyperconjugation for β substituents, which is the reason for opposite signs of hyperfine couplings for ^1H and ^{13}C nuclei.

The relative photo-CIDNP intensities were correlated with calculations of A_{iso} for the relevant TML radicals, see Fig. 6 and Table 2. For this purpose, the photo-CIDNP signals were fitted using Voigt line shapes. For C7α from TMLH, the relative intensity was calculated by integration, as fitting was not possible due to poor resolution of J coupling. The photo-CIDNP resonances of TML^- were correlated to $A_{iso}(TML^\bullet)$, yielding a high correlation of R^2 = 0.9631 and a slope of -0.0222 MHz^{-1}, as illustrated in Fig. 6(a). R^2 is lower than that calculated with ^1H photo-CIDNP (R^2 = 0.9860), which can be attributed to the lower S/N ratio of ^{13}C experiments. The correlation of $A_{iso}(TMLH^{\bullet-})$ with relative photo-CIDNP intensities of TMLH yielded R^2 = 0.9787 and m = 0.0159 MHz^{-1}. Comparable values of R^2 = 0.9850 and 0.0149 MHz^{-1} were found for the correlation of $TMLH_2^\bullet$ (N1). The correlation of $TMLH_2^\bullet$ (N5) yielded a lower correlation of R^2 = 0.9173 and a higher slope of 0.0291 MHz^{-1} compared to the other reduced radical species. Nonetheless, this experiment shows a significantly higher correlation for $TMLH_2^\bullet$ (N5) than the ^1H photo-CIDNP experiment. This indicates that the protonation site N5 exerts a greater influence on ^1H hyperfine couplings than on ^{13}C hyperfine couplings so that the differentiation between different protonation states is easier with ^1H photo-CIDNP thus yielding a lower correlation for $TMLH_2^\bullet$ (N5). Based on the presented photo-CIDNP data we are confident to claim that $TMLH^{\bullet-}$ is not protonated at N5 after radical pair formation. However, further differentiation between $TMLH^{\bullet-}$ and $TMLH_2^\bullet$ (N1) remains speculative based on photo-CIDNP data. For both experiments, a slightly higher correlation for $TMLH_2^\bullet$ (N1) is demonstrated. Nevertheless, the difference in R^2 is not significant enough to reach a definitive conclusion. To the best of our knowledge, no information on pK_A values of 6,7-dimethylated lumazine radicals are available. Therefore, we refer to the pK_A value of TML in its ground state of 0.93 determined for N1.[63] We think it unlikely, that the pK_A for this protonation site in the reduced TML radical is elevated compared to the ground state, so that protonation at pH 13 is possible.

It is noteworthy that the absolute slopes calculated for correlations of the reduced radical species ($TMLH^{\bullet-}$ or $TMLH_2^\bullet$ (N1)) are lower than the one calculated for the oxidized species (for ^1H photo-CIDNP, compare 0.0222 MHz^{-1} and 0.0218 MHz^{-1} with 0.0278 MHz^{-1}. For ^{13}C photo-CIDNP, compare 0.0159 MHz^{-1} and 0.0149 MHz^{-1} with 0.0222 MHz^{-1}). Without any additional polarization loss pathway on a short microsecond timescale which is the time resolution of the experiment, the slopes calculated for both parts of one SCRP should be equal in absolute magnitude.[64] Several effects can be potential sources of polarization loss in TMLH: (i) assuming that $TMLH_2^\bullet$ (N1) is indeed generated during the photo-induced reaction, the subsequent back electron transfer would generate $TMLH_2^+$ in a primary step. This species is expected to

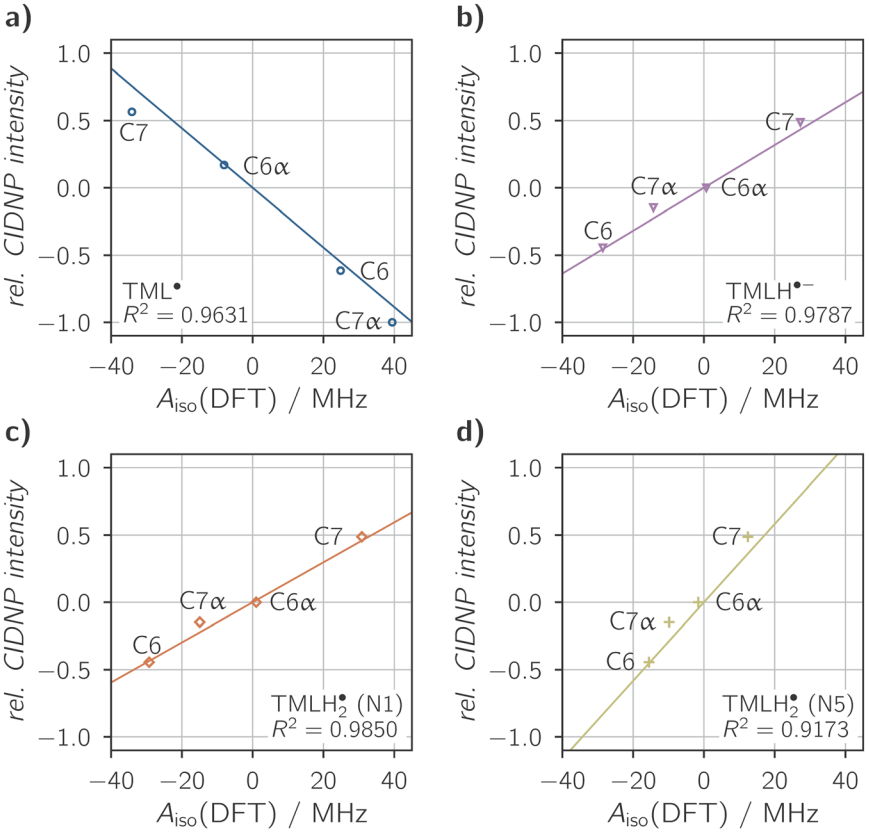

Fig. 6 Linear correlations of the experimentally determined relative ^{13}C photo-CIDNP intensities of [6,6α,7,7α-^{13}C$_4$]TML$^-$ and [6,6α,7,7α-^{13}C$_4$]TMLH with calculated A_{iso} of the relevant radical species: (a) TML• (R^2 = 0.9631, m = −0.0222 MHz^{-1}), (b) TMLH•$^-$ (R^2 = 0.9787, m = 0.0159 MHz^{-1}), (c) TMLH$_2$• (N1) (R^2 = 0.9850, m = 0.0149 MHz^{-1}) and (d) TMLH$_2$• (N5) (R^2 = 0.9173, m = 0.0291 MHz^{-1}). The relative photo-CIDNP intensities of TML$^-$ exhibit a negative proportionality with the respective hyperfine coupling due to Kaptein's rule.[60]

readily deprotonate to form TMLH, which could lead to a dissipation of hyperpolarization into the solvent. (ii) A cancellation due to degenerate electron exchange,

$$^{\downarrow}\text{TMLH}_{\text{red}}{}^{\bullet-} + \text{TMLH} \rightarrow {}^{\downarrow}\text{TMLH} + \text{TMLH}_{\text{red}}{}^{\bullet-}, \quad (1)$$

or (iii) cancellation due to disproportionation of two radicals from the escape route,

$$2\,{}^{\downarrow}\text{TMLH}_{\text{red}}{}^{\bullet-} \rightarrow {}^{\downarrow}\text{TMLH}_2{}^{-} + {}^{\downarrow}\text{TML}^{-}, \quad (2)$$

is possible. In this context, "$^{\downarrow}$" is used to denote photo-CIDNP polarization. Usually, degenerate electron exchange is observed for the electron donor in excess. Nevertheless, both effects have been observed for the electron acceptor riboflavin in a range of 0.2–0.4 mM[65,66] which corresponds to the concentrations of TMLH employed in this study. The speculative process of (iii) would not only deplete TMLH of polarization but also diminish the total polarization of $^{\uparrow}$TML$^-$ to some extent by generating $^{\downarrow}$TML$^-$ of opposite polarization through this second pathway. Given that the loss of polarization is more pronounced in the ^{13}C photo-CIDNP experiment, which utilized a higher concentration of TMLH, it is anticipated that the polarization loss pathway corresponds to either (ii) or (iii) or a combination of both as (ii) and (iii) are concentration dependent.

Table 3 Absolute values of A_{iso} determined for TMLH$_3$•$^+$ (ref. 36) dissolved in CF$_3$COOH as obtained from EPR spectroscopy. These values are compared with A_{iso} of reduced TML radical species calculated by DFT. A_{iso} values are given in MHz. The values of TMLH$_3$•$^+$ were converted from Gauss to MHz using the following equation: A/MHz = $10^{-4}\cdot(g\cdot\mu_B)/h\cdot A$/G. Due to the lack of an experimental value of g for this radical, the g factor of 2.0034 calculated for TMLH•$^-$ was used, see Table S1. As g factors of organic radicals usually show minor variations, the induced error is expected to be negligible

	$\lvert A_{iso}\rvert$/MHz	A_{iso}/MHz		
Nucleus	TMLH$_3$•$^+$ (ref. 36)	TMLH•$^-$	TMLH$_2$• (N1)	TMLH$_2$• (N5)
C6α	2.44	0.69	1.00	−1.60
C7α	18.87	−14.28	−14.94	−9.82
C8α	16.43	−7.77	−7.01	−8.55
H5	22.71			−25.34
N5	20.61	16.37	16.41	14.23
N8	16.43	8.88	7.89	11.39

The investigated TML radical species have not been previously studied and data on other 6,7-dimethyllumazine radicals are scarce. Therefore, the A_{iso} determined cannot be directly compared to literature data. As previously mentioned, Ehrenberg *et al.*[36] investigated a compound, which, in the context of the present publication, can be designated TMLH$_3$•$^+$. This compound corresponds to the reduced TMLH•$^-$ radical

protonated at N1 and N5. The authors determined a number of isotropic hyperfine couplings in absolute values for the nuclei N5, N8, C8α, C7α, C6α and H5. However, a direct comparison with the experimental data of the present study is not feasible as only hyperfine couplings of C6α and C7α are determined in both cases. Consequently, the literature data are tentatively compared to theoretical A_{iso} from DFT which correspond to the real hyperfine structure quite well, see Table 3. The A_{iso} of $TMLH_3^{\bullet+}$ are converted to MHz.

Overall, the A_{iso} values determined for $TMLH_3^{\bullet+}$ follow a similar order of size as A_{iso} determined for all three reduced TML radical species: H5 shows the highest A_{iso} value followed by N5, C7α, N8 and C8α, and C6α. For N8 and C8α, the same value is determined by Ehrenberg *et al.*[36] whereas in this study, $|A_{iso}|$(N8) is greater than $|A_{iso}|$(C8α) for all three radicals. It is anticipated that $TMLH_3^{\bullet+}$ would resemble more closely to one of the TML radical species. However, a direct comparison shows deviations between $TMLH_3^{\bullet+}$ and all three reduced TML radical species. The protonation at both N1 and N5 appears to have a substantial impact on the hyperfine structure of the TML radical. Nevertheless, disparate experimental conditions could account for the differences, as $TMLH_3^{\bullet+}$ was probed in CF_3COOH solution, while the DFT calculations were conducted with a simulation of water solvation.

To further assess whether $TMLH^{\bullet-}$ is protonated, photo-CIDNP experiments employing a higher variety of ^{13}C isotopologues may provide more information, see Table S1 for a list of all A_{iso} values of the TML radical species. For example, A_{iso}(C2) is expected to be affected by protonation at N1, which may be discernible by photo-CIDNP. It is not anticipated that valuable information will be obtained from ^{15}N photo-CIDNP, as the isotropic hyperfine interactions of ^{15}N nuclei do not exhibit significant variation between the protonation states of the $TMLH^{\bullet-}$ radical. A comparable challenge in differentiating between protonation states was encountered in studies of the 5-deazaflavin radical through photo-CIDNP employing 5-deazaflavin mononucleotide[67] and demethylated 5-deazariboflavins.[68] Contrary to flavin radicals, protonation at N5 is impeded by exchanging N by C–H at this position. The second protonation site of 5-deazariboflavin, N1, does not significantly alter the hyperfine structure of the radical, so that both protonation states share a similar photo-CIDNP spectrum. In this regard, flavin and 6,7-dimethyllumazine radicals demonstrate similar behavior.

3.3 Reaction mechanism of TML

With these new findings based on ^1H and ^{13}C photo-CIDNP, we establish a modified reaction cycle of the photo-induced disproportionation reaction of TMLH and TML^-, see Fig. 7. TMLH is photo-excited into an excited triplet state[11] *via* intersystem crossing (ISC) and undergoes one-electron reduction from TML^-. The resulting SCRP $[TMLH^{\bullet-}\cdots TML^{\bullet}]$ may undergo direct recombination to form the initial compounds. Alternatively, protonation of $TMLH^{\bullet-}$ at N1 results in the generation of a neutral SCRP $[TMLH_2^{\bullet}\cdots TML^{\bullet}]$. Subsequent

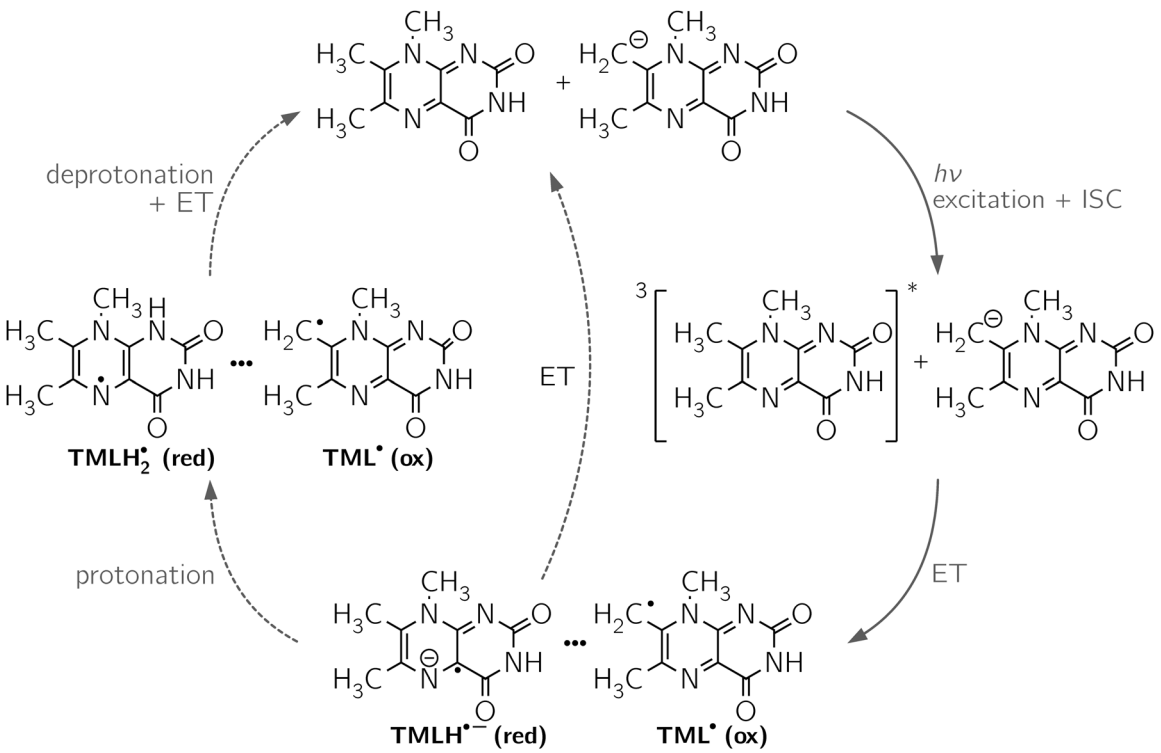

Fig. 7 Reaction mechanism of the photo-induced disproportionation of TMLH in basic solution. Initially, TMLH is excited into a triplet state following intersystem crossing (ISC).[11] Electron transfer (ET) from TML^- results in the formation of the SCRP $[TMLH^{\bullet-}$(red)$\cdots TML^{\bullet}$(ox)]. Thereafter, two pathways are possible: either the SCRP directly decays back to TMLH and TML^- or $TMLH^{\bullet-}$ is protonated at N1 by the solvent followed by the decay of the SCRP *via* deprotonation and ET. The available data does not allow for a clear distinction between these two pathways.

to deprotonation and electron back transfer, the initial compounds are regenerated. The experiments conducted have not yielded sufficient data to distinguish between the two possibilities.

This study provides evidence that 6,7-dimethyllumazine anions are capable of undergoing light-induced dismutations. This finding may have implications for future studies on the mechanism of riboflavin biosynthesis from DMRL[69] and on the photocycle of lumazine-containing proteins. It should be noted that the photochemical reactivity of a protein-bound cofactor may be impacted by the protein environment. Therefore, the electron transfer properties of bound 6,7-dimethyllumazines may deviate from the findings of this study. The study by Paulus *et al.*[35] on DMRL and riboflavin bound to lumazine protein exemplifies this aspect. The authors probed the kinetics of photoreduction of DMRL in solution and incorporated in different mutants of lumazine protein and found significant deviations, notably a slower photoreduction of the cofactor and a higher accumulation of the DMRL radical in the lumazine protein.

3.4 Mulliken spin densities of TML radicals

The experimental determination of the ^{1}H and ^{13}C hyperfine structure has revealed fundamental differences between the oxidized ($TML^{\bullet}$) and reduced ($TMLH^{\bullet-}$ or $TMLH_2^{\bullet}$ (N1)) radical species. A comprehensive discussion of these disparities can be facilitated by the spin polarization model by Karplus and Fraenkel.[70] This model offers a rationalization of isotropic hyperfine interaction and spin density of carbons in π-based radicals. The hyperfine coupling of a carbon nucleus is not only affected by the spin density located on the nucleus itself, but also modulated in the opposite direction by spin densities of adjacent nuclei.

To account for the origin of the different hyperfine structures of the TML radical species, Mulliken spin populations were calculated using DFT, see Fig. 8 for a graphical representation and Fig. S2 for a bar chart visualization. When not determined experimentally, A_{iso} are calculated by DFT, see Table S1.

In summary, the left side of the ^{13}C and ^{15}N framework in TML is predominantly affected in their spin population distribution when comparing oxidized and reduced TML radical, partly to a considerable extent. The different oxidation states show sign flips and substantially different magnitudes of spin population. The right side of the TML structure is affected less significantly due to small spin populations. For this reason, these nuclei are omitted in the following detailed discussion of how the differences in hyperfine coupling result from the presented Mulliken spin populations.

In the reduced TML radical, with ($TMLH_2^{\bullet}$ (N1)) or without protonation at N1 ($TMLH^{\bullet-}$), N5 carries the highest spin population with about 37%. In both species, A_{iso}(C4a) exhibits a medium-sized negative hyperfine coupling, despite its positive spin population, due to strong polarization by N5.

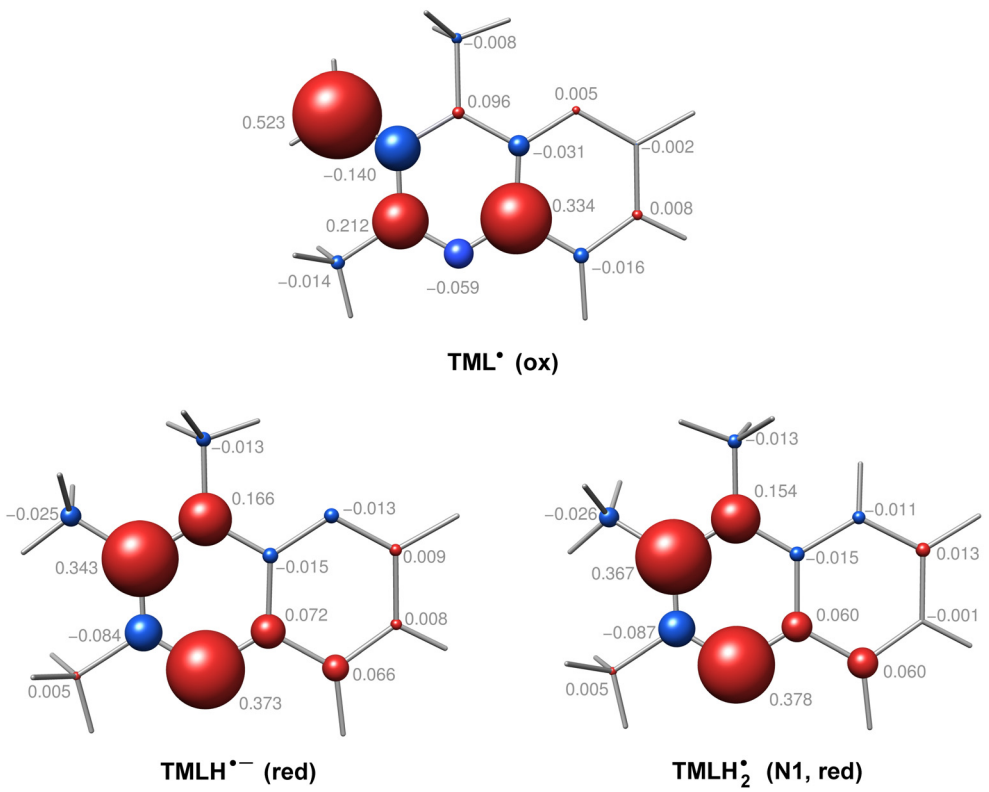

Fig. 8 Graphical representation of Mulliken spin populations of the carbon and nitrogen nuclei in the lumazine moieties of $TML^{\bullet}$, $TMLH^{\bullet-}$ and $TMLH_2^{\bullet}$ (N1) as obtained from DFT calculations using B3LYP/EPR-II. A listing and a bar chart representation of all values is provided in Table S2 and Fig. S2.

Conversely, C6 exhibits a pronounced negative hyperfine coupling. This is due to a moderately negative spin density of C6. Additionally, the adjacent N5 and C7 exert a polarizing effect through their high positive spin densities. C7 itself exhibits a strong positive hyperfine coupling. The nucleus has a high positive spin density of 34–37%. The neighboring nuclei, C6 and N8, exhibit moderate negative and positive spin densities, so that their polarization of C7 is averaged. The methyl groups 6α, 7α and 8α are not part of the π system. Consequently, their spin population is due to direct polarization from their adjacent π nuclei as established by McConnell, Chesnut and Heller.[61,62] The methyl carbons exhibit smaller and opposite hyperfine couplings compared to their neighboring π nuclei. This is particularly evident in C6α, which exhibits an A_{iso} value lower than 1 MHz.

The formal deprotonation of C7α of $TMLH^{\bullet-}$ results in the formation of the oxidized radical $TML^{\bullet}$. Its spin density pattern is predominantly influenced by C7α, which is part of the π network. Consequently, this leads to a significant reduction and inversion of the spin population of N5. C4a exhibits a high amount of positive spin density. Together with the polarizing effect of the adjacent N5, an exceptionally high positive hyperfine coupling results. Similarly, C6 exhibits a high positive hyperfine coupling resulting from its positive spin population and the polarization by moderate negative spin populations of N5 and C7. Despite the relatively modest negative spin population of C7, the combined polarization by C7α, C6 and N8, each exhibiting moderate to high positive spin populations, culminate in a pronounced negative hyperfine coupling. The equally strong, positive hyperfine coupling of C7α can be attributed to its substantial spin population of 52% as well as a slight polarizing effect of C7.

4 Conclusions

In this study, we have investigated the photo-induced disproportionation reaction of TML using a combination of NMR, photo-CIDNP spectroscopy and DFT calculations. Our results provide profound insights into the structure of the TML anion and the hyperfine structure of TML radicals in different oxidation states. Analysis of a (^{1}H,^{1}H)-NOESY spectrum revealed that TML^{-} retains a rigid structure. The C7–C7α bond corresponds to an exomethylene, thus re-evaluating the findings of a previous study.[11] These observations are supported by temperature-dependent NMR and a potential energy surface scan of the H7α′–C7α–H7α″ angle, which further excludes the presence of a carbanion configuration.

Photo-CIDNP spectroscopy confirmed a transient SCRP consisting of an oxidized and reduced TML radical formed in a unique disproportionation reaction of neutral and anionic TML. Analysis of the CIDNP resonances reveals substantial differences in the oxidized and reduced TML radicals. The experimental hyperfine coupling constants are in strong agreement with DFT calculations. Thus, the TML radicals formed are the oxidized $TML^{\bullet}$ and the reduced $TMLH^{\bullet-}$ or $TMLH_2^{\bullet}$ protonated at N1. The formation of a $TMLH_2^{\bullet}$ radical protonated at N5 as described previously[11] can be excluded. The analyzed hyperfine structures are rationalized on the basis of calculations of the spin population distribution in both radical species. Overall, our results contribute to a deeper understanding of 6,7-dimethyllumazine redox chemistry, particularly in the context of one-electron transfer processes. As the oxidized TML radical corresponds to a formerly unknown oxidation state of lumazines, this study provides an in-depth investigation of its electronic structure. The results can be used to derive the hyperfine structure of DMRL radicals which are not readily accessible by photo-CIDNP spectroscopy. This contribution may have implications for further studies on lumazine-containing proteins and the role of lumazines in electron transfer reactions in biological systems.

Author contributions

Conceptualization: S. P., A. B., M. F. and S. W.; data curation: S. P., J. C.; formal analysis: S. P.; funding acquisition: M. F. and S. W.; investigation: S. P. and J. C.; methodology: S. P. and S. W.; project administration: M. F. and S. W.; resources: S. P., J. C., B. I., A. B., M. F., S. W.; software: S. P.; supervision: A. B., M. F. and S. W.; validation: S. P. and J. C.; visualization: S. P.; writing – original draft: S. P., B. I. and S. W.; writing – review & editing: B. I., A. B. and M. F.

Conflicts of interest

There are no conflicts to declare.

Data availability

The data supporting this article have been included as part of the SI. Supplementary information is available: input and results from density functional theory calculations, additional NMR data, full description of chemical synthesis. See DOI: **https://doi.org/10.1039/d5cp02105g**

Acknowledgements

The authors thank Ursula Friedrich for the purification of the samples. SW thanks the SIBW/DFG for financing NMR instrumentation that is operated within the MagRes Center of the Albert-Ludwigs-Universität Freiburg (Germany). SW and MF acknowledge financial support from the Deutsche Forschungsgemeinschaft (DFG) (project number 459493567: WE 2376/12-1 and FI824/13-1).

Notes and references

1 W. Kaim, B. Schwederski, O. Heilmann and F. M. Hornung, *Coord. Chem. Rev.*, 1999, **182**, 323–342.
2 B. J. Daniels, F. F. Li, D. P. Furkert and M. A. Brimble, *J. Nat. Prod.*, 2019, **82**, 2054–2065.

3 R. Kuhn and A. H. Cook, *Ber. Dtsch. Chem. Ges. A*, 1937, **70**, 761–768.
4 T. Paterson and H. C. S. Wood, *J. Chem. Soc. D*, 1969, 290.
5 W. Pfleiderer, R. Mengel and P. Hemmerich, *Chem. Ber.*, 1971, **104**, 2273–2292.
6 W. Pfleiderer, J. W. Bunting, D. D. Perrin and G. Nübel, *Chem. Ber.*, 1966, **99**, 3503–3523.
7 D. H. Bown, P. J. Keller, H. G. Floss, H. Sedlmaier and A. Bacher, *J. Org. Chem.*, 1986, **51**, 2461–2467.
8 J. M. McAndless and R. Stewart, *Can. J. Chem.*, 1970, **48**, 263–270.
9 R. L. Beach and G. W. E. Plaut, *Biochemistry*, 1970, **9**, 760–770.
10 R. L. Beach and G. W. E. Plaut, *J. Org. Chem.*, 1971, **36**, 3937–3943.
11 J. Wörner, J. Chen, A. Bacher and S. Weber, *Magn. Reson.*, 2021, **2**, 281–290.
12 R. A. Harvey and G. W. E. Plaut, *J. Biol. Chem.*, 1966, **241**, 2120–2136.
13 G. Plaut, *J. Biol. Chem.*, 1963, **238**, 2225–2243.
14 H. Wacker, R. A. Harvey, C. H. Winestock and G. Plaut, *J. Biol. Chem.*, 1964, **239**, 3493–3497.
15 R. L. Beach and G. W. E. Plaut, *J. Am. Chem. Soc.*, 1970, **92**, 2913–2916.
16 M. Cushman, D. A. Patrick, A. Bacher and J. Scheuring, *J. Org. Chem.*, 1991, **56**, 4603–4608.
17 A. Talukdar, B. Illarionov, A. Bacher, M. Fischer and M. Cushman, *J. Org. Chem.*, 2007, **72**, 7167–7175.
18 Y. Zhang, B. Illarionov, A. Bacher, M. Fischer, G. I. Georg, Q.-Z. Ye, D. Vander Velde, P. E. Fanwick, Y. Song and M. Cushman, *J. Org. Chem.*, 2007, **72**, 2769–2776.
19 E. Morgunova, B. Illarionov, S. Saller, A. Popov, T. Sambaiah, A. Bacher, M. Cushman, M. Fischer and R. Ladenstein, *Acta Crystallogr., Sect. D: Struct. Biol.*, 2010, **66**, 1001–1011.
20 Y. Zhang, B. Illarionov, E. Morgunova, G. Jin, A. Bacher, M. Fischer, R. Ladenstein and M. Cushman, *J. Org. Chem.*, 2008, **73**, 2715–2724.
21 R. Gast, I. R. Neering and J. Lee, *Biochem. Biophys. Res. Commun.*, 1978, **80**, 14–21.
22 E. D. Small, P. Koka and J. Lee, *J. Biol. Chem.*, 1980, **255**, 8804–8810.
23 J. Lee, *Biophys. Chem.*, 1993, **48**, 149–158.
24 M. S. Titushin, Y. Feng, J. Lee, E. S. Vysotski and Z.-J. Liu, *Protein Cell*, 2011, **2**, 957–972.
25 S. Weber, *Biochim. Biophys. Acta*, 2005, **1707**, 1–23.
26 I. Chaves, R. Pokorny, M. Byrdin, N. Hoang, T. Ritz, K. Brettel, L.-O. Essen, G. T. J. van der Horst, A. Batschauer and M. Ahmad, *Annu. Rev. Plant Biol.*, 2011, **62**, 335–364.
27 Y. Geisselbrecht, S. Frühwirth, C. Schroeder, A. J. Pierik, G. Klug and L.-O. Essen, *EMBO Rep.*, 2012, **13**, 223–229.
28 F. Zhang, P. Scheerer, I. Oberpichler, T. Lamparter and N. Krauß, *Proc. Natl. Acad. Sci. U. S. A.*, 2013, **110**, 7217–7222.
29 Z. Ren, W. Kang, S. Gunawardana, K. Bowatte, K. Thoulass, G. Kaeser, N. Krauß, T. Lamparter and X. Yang, *Cell Rep. Phys. Sci.*, 2023, **4**, 101297.
30 R.-X. He and D.-W. Zha, *J. Electroanal. Chem.*, 2017, **791**, 103–108.
31 R. K. Kar, A.-F. Miller and M.-A. Mroginski, *Wiley Interdiscip. Rev.: Comput. Mol. Sci.*, 2022, **12**, e1541.
32 P. N. Moorthy and E. Hayon, *J. Phys. Chem.*, 1975, **79**, 1059–1062.
33 G. Harzer and S. Ghisla, *Chemistry and Biology of Pteridines: International Symposium Proceedings*, Elsevier, Amsterdam, 1979, pp. 37–42.
34 G. Wetzel and S. Ghisla, *Chemistry and Biology of Pteridines: 7 St. Andrews, Scotland, September 21-24, 1982*, De Gruyter, Berlin, Boston, 1983, pp. 693–698.
35 B. Paulus, B. Illarionov, D. Nohr, G. Roellinger, S. Kacprzak, M. Fischer, S. Weber, A. Bacher and E. Schleicher, *J. Phys. Chem. B*, 2014, **118**, 13092–13105.
36 A. Ehrenberg, P. Hemmerich, F. Müller and W. Pfleiderer, *Eur. J. Biochem.*, 1970, **16**, 584–591.
37 J. Westerling, H. I. X. Mager and W. Berends, *Tetrahedron*, 1977, **33**, 2587–2594.
38 S.-C. Tu, H. I. X. Mager, R. Shao, K. W. Cho and L. Xi, *Flavins and Flavoproteins 1990, Proceedings of the Tenth International Symposium*, De Gruyter, Berlin, New York, 1991, pp. 253–260.
39 S. G. Ballard and D. C. Mauzerall, *J. Phys. Chem.*, 1976, **80**, 341–351.
40 M. Insińska-Rak and M. Sikorski, *Chem. – Eur. J.*, 2014, **20**, 15280–15291.
41 P. F. Heelis, B. J. Parsons, G. O. Phillips and A. J. Swallow, *J. Phys. Chem.*, 1986, **90**, 6833–6836.
42 Y. Okuno and S. Cavagnero, *eMagRes*, 2017, **6**, 283–314.
43 O. B. Morozova and K. L. Ivanov, *ChemPhysChem*, 2019, **20**, 197–215.
44 J. Eills, D. Budker, S. Cavagnero, E. Y. Chekmenev, S. J. Elliott, S. Jannin, A. Lesage, J. Matysik, T. Meersmann, T. Prisner, J. A. Reimer, H. Yang and I. V. Koptyug, *Chem. Rev.*, 2023, **123**, 1417–1551.
45 J. Bargon, H. Fischer and U. Johnsen, *Z. Naturforsch., A*, 1967, **22**, 1551–1555.
46 J. Bargon and H. Fischer, *Z. Naturforsch., A*, 1967, **22**, 1556–1562.
47 H. R. Ward and R. G. Lawler, *J. Am. Chem. Soc.*, 1967, **89**, 5518–5519.
48 T. Masuda, *Pharm. Bull.*, 1956, **4**, 375–381.
49 T. L. Hwang and A. J. Shaka, *J. Magn. Reson., Ser. A*, 1995, **112**, 275–279.
50 N. Pompe, J. Chen, B. Illarionov, S. Panter, M. Fischer, A. Bacher and S. Weber, *J. Chem. Phys.*, 2019, **151**, 235103.
51 N. Pompe, B. Illarionov, M. Fischer, A. Bacher and S. Weber, *J. Phys. Chem. Lett.*, 2022, **13**, 5160–5167.
52 F. Neese, *Wiley Interdiscip. Rev.: Comput. Mol. Sci.*, 2012, **2**, 73–78.
53 F. Neese, *Wiley Interdiscip. Rev.: Comput. Mol. Sci.*, 2018, **8**, e1327.
54 W. J. Schreier, I. Pugliesi, F. O. Koller, T. E. Schrader, W. Zinth, M. Braun, S. Kacprzak, S. Weber, W. Römisch-Margl, A. Bacher, B. Illarionov and M. Fischer, *J. Phys. Chem. B*, 2011, **115**, 3689–3697.
55 P. J. Stephens, F. J. Devlin, C. F. Chabalowski and M. J. Frisch, *J. Phys. Chem.*, 1994, **98**, 11623–11627.

56 F. Weigend and R. Ahlrichs, *Phys. Chem. Chem. Phys.*, 2005, **7**, 3297–3305.
57 F. Weigend, *Phys. Chem. Chem. Phys.*, 2006, **8**, 1057–1065.
58 V. Barone and M. Cossi, *J. Phys. Chem. A*, 1998, **102**, 1995–2001.
59 W. Kutzelnigg, U. Fleischer and M. Schindler, *Deuterium and Shift Calculation*, Springer, Berlin, Heidelberg, 1990, pp. 165–262.
60 R. Kaptein, *Chem. Commun.*, 1971, 732–733.
61 H. M. McConnell and D. B. Chesnut, *J. Chem. Phys.*, 1958, **28**, 107–117.
62 C. Heller and H. M. McConnell, *J. Chem. Phys.*, 1960, **32**, 1535–1539.
63 R. Stewart, R. Srinivasan and S. J. Gumbley, *Can. J. Chem.*, 1981, **59**, 2755–2765.
64 O. B. Morozova, K. L. Ivanov, A. S. Kiryutin, R. Z. Sagdeev, T. Köchling, H.-M. Vieth and A. V. Yurkovskaya, *Phys. Chem. Chem. Phys.*, 2011, **13**, 6619–6627.
65 R. Kaptein, K. Dijkstra, F. Müller, C. G. van Schagen and A. J. W. G. Visser, *J. Magn. Reson.*, 1978, **31**, 171–176.
66 P. J. Hore, E. R. P. Zuiderweg, R. Kaptein and K. Dijkstra, *Chem. Phys. Lett.*, 1981, **83**, 376–383.
67 J. Wörner, S. Panter, B. Illarionov, A. Bacher, M. Fischer and S. Weber, *Angew. Chem., Int. Ed.*, 2023, **62**, e202309334.
68 S. Panter, A. Ayekoi, J. Tesche, J. Chen, B. Illarionov, A. Bacher, M. Fischer and S. Weber, *Int. J. Mol. Sci.*, 2024, **25**, 848.
69 M. Breugst, A. Eschenmoser and K. N. Houk, *J. Am. Chem. Soc.*, 2013, **135**, 6658–6668.
70 M. Karplus and G. K. Fraenkel, *J. Chem. Phys.*, 1961, **35**, 1312–1323.